An Optical Router for Quantum Communication

Student Name: Li Jiaqi

Student ID: A0253911J

Supervisor name: Prof. Christian Kurtsiefer

Co-Supervisor name: Dr. Hou Shun POH

A Research Project Report (PC5286) Submitted for the

M.Sc. in Physics

Department of Physics,

National University of Singapore. AY2023/2024

Acknowledgments

I would like to express my sincere gratitude to my mentor, Professor Christian Kurtsiefer, for his unwavering support and professional guidance throughout this project. Special appreciation goes to my co - supervisor, Hou Shun POH, for his patient guidance and continuous support, significantly enhancing my experimental skills and theoretical knowledge and providing a profound insight into this project. I also extend my thanks to all my lab mates for their assistance in facilitating my rapid integration into the lab.

Furthermore, I want to express my appreciation to my friends, especially Mo Cuiying, Yang Chen, and Li Huangxin, for their companionship during my time in Singapore. Lastly, I want to convey my heartfelt thanks to my family for their steadfast support and encouragement, enabling me to make courageous choices in shaping my own path in life.

Abstract

With the development of quantum communication technology, the optical router, as a component in quantum information transmission, is crucial for achieving an efficient and reliable quantum communication network. This study aims to conduct in-depth research on key components of optical routers used in quantum communication and evaluate their performance and potential applications through experimental assessment. It primarily focuses on exploring the Galvo scanning system for controlling beam steering and studying the coupling between fiber-to-fiber free space. In this paper, the working principle and structure of the Galvo scanning system are described in detail. Through precise experimental design and measurement, the position accuracy, repeatability and dynamic characteristics of the system are evaluated comprehensively. Additionally, the knife-edge method is utilized to measure the diameter of the Gaussian beam, obtaining the beam profile and essential data such as the size and position of the beam waist, to characterize different types of fiber collimators. Furthermore, the optimal coupling distance from the fiber to the collimator is explored.

This paper presents a comprehensive evaluation of key components in optical routers for quantum communication in terms of performance and application. These results are of great significance to further optimize the design and performance of optical routers, provide valuable insights for the development and practical application of quantum communication networks, and lay a foundation for future research.

Keywords: Quantum key distribution network, Optical router, Free-space optical switch, Galvo scanning system, Collimator

Contents

Chapter 1 Introduction

1.1 Quantum Key Distribution

Quantum communication is a type of communication that uses the principles of quantum mechanics to transmit information. Compared with traditional communications, quantum communications use qubits as the basic unit of information. Using the coherence and indivisibility of quantum states for the transmission of information, efficient and secure information transmission can be achieved. In 1984, Bennett et al.[1] proposed quantum key distribution (QKD), which is a secure communication method that enables two parties to generate a shared secret key. Both parties can determine whether there is eavesdropping by the information they have and can use “One-time pad” (OTP) to encrypt and decrypt classical messages to be transmitted, achieving unconditional security in principle.

Due to its security and high efficiency, quantum secure communication based on quantum key distribution has become a hotspot of theoretical research and application in the field of quantum communication, as well as the earliest researched and most widely applied technology, which has flourished in the past 40 years.

1.2 Quantum Key Distribution Network

The non-cloning theorem[2] states that it is impossible to create independent and identical copies of any unknown quantum state, so quantum key distribution is essentially a "point-to-point" protocol. To realize multi-user communication, the point-to-point QKD is extended to construct Quantum Key Distribution network (QKDN). Therefore, the QKD networking technology has become a new research target.

A quantum network consists of fixed nodes that store, transmit or process quantum information and a network component that allows information to be exchanged between nodes over extended distances. The network part is implemented using photons as information carriers that travel over long distances with low loss while retaining the quantum information encoded in them. The network part is implemented using photons as information carriers that travel over long distances with low loss while retaining the quantum information encoded in them. Photons can be transmitted over existing fibre optic networks used for classical communications to reduce costs[8]. But there needs to be a transparent optical path between both parties to preserve the quantum state of the photons for QKD. These optical path routings can be achieved with optical switches.

There are three primary types of QKD network building schemes: classical optics-based QKD networks, trusted relay-based QKD networks, and quantum relay-based QKD networks.

1.2.1 QKD Networking technology based on classical optical devices

Networking solutions based on classical optical devices considers the use of classical optical devices such as beam splitters, optical switches, and wavelength division multiplexers to multiplex the transmission of multiple quantum channels in order to construct a QKD network[3].

In 1994, Townsend et al. proposed a networking scheme based on optical beam splitter[5], in which the transmitter is divided into N beams by 1×N optical beam splitter, which enter into N receivers respectively for quantum key distribution. And different network topologies can be chosen, such as star topology and ring topology. The advantages of the optical beam splitter based networking scheme are low cost, easy to build and no active switching. However, the disadvantage is that it is not extensible and the maximum transmission distance is limited by the loss of the quantum channel, i.e., as the number of users increases, the transmission rate becomes lower and the loss increases. According to the example mentioned by Hou Jia in his research on quantum key distribution networking schemes[4], when the number of users is raised to 32, the

insertion loss of the optical beam splitter is already as high as 16dB, which is equivalent to using 80km of optical fibre for transmission.

QKD network can also be achieved based on optical switches, where multiple QKD terminals will build quantum channels through optical switches that can be actively switched. Optical switches have low insertion loss and scalability compared to beam splitters, enabling selective connectivity of quantum channels. Since its insertion loss is equal to the insertion loss of the point-to-point QKD at the time of connectivity, it does not increase with the size of users. If we continue to compare with the previously mentioned example, the insertion loss using an optical beam splitter is 16 times higher than that of an optical switch for the same number of users.

There is also a more mainstream scheme for implementing QKD networks based on WDMs, i.e., using tunable lasers at the transmitter side and using different wavelengths for quantum key distribution for different users. The insertion loss of WDM in an optical router is between that of an optical switch and an optical beam splitter. WDM has improved scalability but at the same time places higher demands on the number of wavelengths. The networking scheme based on WDM can achieve a full-time all-pass network with multiple nodes. By combining multiple WDMs to build a quantum router and setting up the receive wavelength and transmit wavelength of each node, the desired function can be achieved[4].

In networking schemes based on classical optics, the insertion loss due to optics can limit the maximum transmission distance of QKDs, but security is good, cost is low, and it can be achieved with existing technology. Optical beam splitters have the most insertion loss and optical switches have the least insertion loss. In terms of scalability, optical switches have better scalability compared to WDM and have more potential for quantum communication between multiple users. In terms of QKD network connectivity, optical switches can achieve selective interworking and WDM can achieve full-time interworking. As active devices, optical switches require active control. Classical optics can be considered for building QKD networks when the length of safe communication distance is not very long. In the case of longer transmission distance requirements, such as wide-area quantum key distribution networks, we need to consider constructing a relay QKD network.

1.2.2 QKD Networking technology based on trusted relay

Losses caused by the transmission medium will limit the maximum transmission distance that can be achieved by a quantum key distribution network. In classical communications, signals can be amplified by technical means, such as the use of amplifiers. However, in quantum communication, the non-cloning theorem will prohibit the use of devices such as amplifiers[3], so the use of relay technology is considered to achieve long-distance communication.

In 2002, Elloitt et al. proposed the use of trusted relay techniques to construct QKD networks[6]. If the sender is set to be Alice and the receiver is Bob, there is a trusted relay node between the two parties. Alice and the repeater generate the key k_1 through QKD and Bob and the repeater generate the key k_2 through QKD. Alice encrypts the key k_{AB} which needs to be shared with Bob through k_1 using one-time pad (OTP) and sends the final key to the node. The trusted relay node can decrypt k_{AB} and encrypt it with k_2 and send it to Bob. Bob only needs to decrypt to get k_{AB}.

Theoretically, it is possible to transmit quantum signals between these relay nodes securely using OTP, but first it is important to make sure that the relay nodes are reliable and safe. Trusted relay nodes use encryption to protect key information and follow theoretically secure protocols, which is a necessary component of building a secure and trusted quantum communication network.

On the other hand, a free-space channel can be employed in place of the optical fiber that is now being used to transmit signals, which will increase the maximum communication distance and decrease the loss brought on by the transmission medium. For example, satellite quantum communication networks use satellites as relay nodes to transmit quantum information through free space.

1.2.3 QKD Networking technology based on quantum relay

Briegel et al. first proposed the concept of quantum repeaters[7], which, unlike classical repeaters, are based on quantum entanglement and use techniques such as entanglement swapping and entanglement purification to achieve long-distance relay extension of quantum entanglement effects.

Assuming that Charles is located between Alice and Bob, Charles has a shorter distance from Alice, so he can establish entanglement between them; similarly, Bob and Charles can also establish entanglement. Charles shares one EPR pair E_1 with Alice and another EPR pair E_2 with Bob. Charles can then perform Bell measurements on the two half-pairs in his hand and broadcast his measurements. Based on Charles' measurements, Alice and Bob can convert the two photons into EPR pairs by performing local operations. This establishes long-distance entanglement between Alice and Bob by sacrificing an EPR pair.

The advantage of a quantum relay over a trusted relay is that it is highly secure. Since the quantum relay does not contain information about the final key, there is no need to ensure that the quantum relay is trusted. However, quantum relay has a high

demand for extremely fine quantum memory (QM), etc., which is currently technically difficult to achieve.

1.3 Propose of the Project

In this project, the main objective is to investigate the feasibility of a free-space optical switch optimized quantum traffic. The research is divided into three main parts: a survey of commercial optical switches and a comparison of their insertion loss with free-space optical switches; Ascertaining the feasibility of using galvo-driven mirrors for beam steering, i.e., measuring the accuracy and repeatability of the mirrors; and investigating and optimizing fibre-to-fibre free-space coupling.

Chapter 2 Optical Switch

Optical switches are used to control the routing and switching of optical signals, which can be sent from an input to a specified output in response to an incoming control signal. Most common optical switches use mechanical actuation, thermal effects in the optical fibre, waveguide effects or the refractive index of light by an electric field to switch the optical signal. In the following sections, the research will focus on traditional mechanical optical switches, MEMS optical switches and free-space optical switches, and compare the insertion loss of commercial optical switches and free-space optical switches.

2.1 Mechanical Optical Switch

A Mechanical Optical Switch uses mechanical movement to switch an optical signal. It usually consists of miniature mechanical components, such as rotating or moving parts, that switch the beam from one input port to one or more output ports. More widely used are 1×2 and 2×2 mechanical optical switches.

There are three general techniques to achieve optical switching: using prisms, using mirrors and moving optical fibres[9]. The working principle is basically the same and can be summarised as the use of an external drive, such as a motor or actuator, to

move a prism, mirror or optical fibre to switch the beam path. For the first two technologies, the input and output are fixed, and only the prisms and mirrors need to be moved to change the path of the beam, which has become a widely used commercial product. The moving fibre technique is based on fixing the fibre at one end and moving the fibre at the other end so that the beam goes to a different output.

Mechanical optical switches have relatively mature technology, simpler manufacturing and operation, lower cost, and low insertion loss. However, mechanical optical switches also have certain limitations and drawbacks, one is that the switching speed of mechanical optical switches is slow compared to other optical switches. Since the movement of mechanical components requires a period of time, the switching speed is limited and is not suitable for application scenarios with high speed and high real-time requirements. Second, mechanical optical switches usually require a large volume and complex structure to achieve beam path switching. For highly integrated optical systems, mechanical optical switches may be less suitable. Third, the performance of mechanical optical switches is susceptible to external vibration and shock. In industrial environments or mobile applications, mechanical optical switches may suffer from erratic path switching or signal loss due to shifting or misalignment of mechanical components.

2.2 MEMS Optical Switch

MEMS (Micro Electro-Mechanical System) optical switches usually consist of micromirrors, microdrivers and optical fibres. The micromirror is the most critical component, which reflects or transmits optical signals in different positions. By applying an external voltage or current, the microdriver can cause a movement of the micromirror that changes the path of the optical signal. MEMS optical switches have been classified into optical path obscuring type, mobile fibre docking type and micromirror reflecting type according to their functional implementation[10]. In this section, the micromirror reflection type optical switch will be used as an example to introduce the different dimensions of the optical switch.

The core component of a 2D MEMS optical switch is an array of micro-bent or micro-rotated mirrors. These mirrors are typically made of metal or multilayer thin-film materials with high reflectivity and optical stability. They are mounted on micro-cantilevers or micro-rotors that can undergo small displacements and rotations in response to electric fields or forces. By controlling the rotation of the mirrors, it is possible to connect the beam to a specified output. Fig. 1 shows a 2×2 2D MEMS optical switch. The light beam is injected into the 2D optical switch from the input, and when the micro-reflector is not activated, the micro-mirror will remain horizontal and the beam passes directly through the micro-mirror. When a specific micro-reflector is activated, the micromirror becomes vertical. The beam hits the micromirror and is

reflected to the corresponding output port. By adjusting the position of the micro mirrors, the optical path can be input and output from the desired ports.

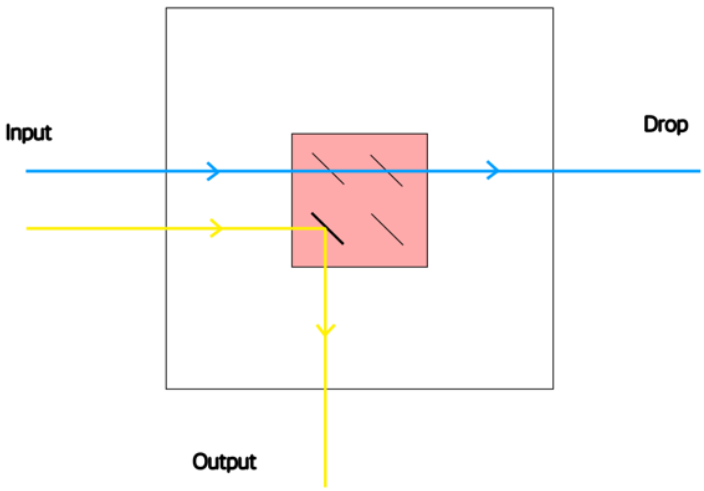

Fig. 1. Two-dimensional MEMS optical switch.

Two-dimensional MEMS optical switches are easy to operate and control. Since the micro-reflector has only two states, it can be controlled using simple digital signals, and the optical switch only needs to be given a voltage to drive the movement of the micro-reflector. However, the disadvantage is that if it is expanded into a large optical switch array, the selection of different input and output ports will result in a large difference in transmission distance, which means that the insertion loss will also be significantly different. Therefore, 2D MEMS optical switches are not suitable for use in larger scale optical switch arrays[10].

Three-dimensional MEMS optical switches have similar implementation principles to two-dimensional MEMS optical switches, but three-dimensional MEMS optical switches are a more complex and advanced structure. They allow the micro-reflector to rotate in two axes in both directions, rather than being limited to just two states, on and off. The advantage is that an array of optical switches of the same size as a 2D MEMS optical switch can be realized using fewer mirrors. However, the 3D optical switch requires precise control of the mirror position, which makes the design of the structure and control circuit of the 3D optical switch encounter more difficult problems.

2.3 Free space Optical Switch

Free-space optical switches are used to switch and route optical signals in free space. The beam in the optical fibre is collimated into free space, where it is processed and switched by the free-space optical switch and output to the designated port. The free-space optical switch achieves higher optical signal transmission bandwidth and lower insertion loss due to the lower loss caused by the transmission of the light beam in the air medium. Compared with mechanical optical switches and MEMS optical switches, free-space optical switches have good scalability and flexibility, which can be optimised and adjusted, and have important applications in optical communication and optical networks.

2.4 Comparison of Insertion Losses

In quantum communication, low insertion loss and preservation of polarization degrees of freedom for quantum information encoding are the most important criteria. In this paper, the insertion loss of nearly 70 commercial mechanical optical switches and MEMS optical switches from more than ten manufacturers are collected. On the one hand, it is to understand the relationship between the number of quantum channels and insertion loss of commercial optical switches, and on the other hand, it can be compared with the free-space optical switches realized based on galvo mirror system, as shown in Fig. 2.

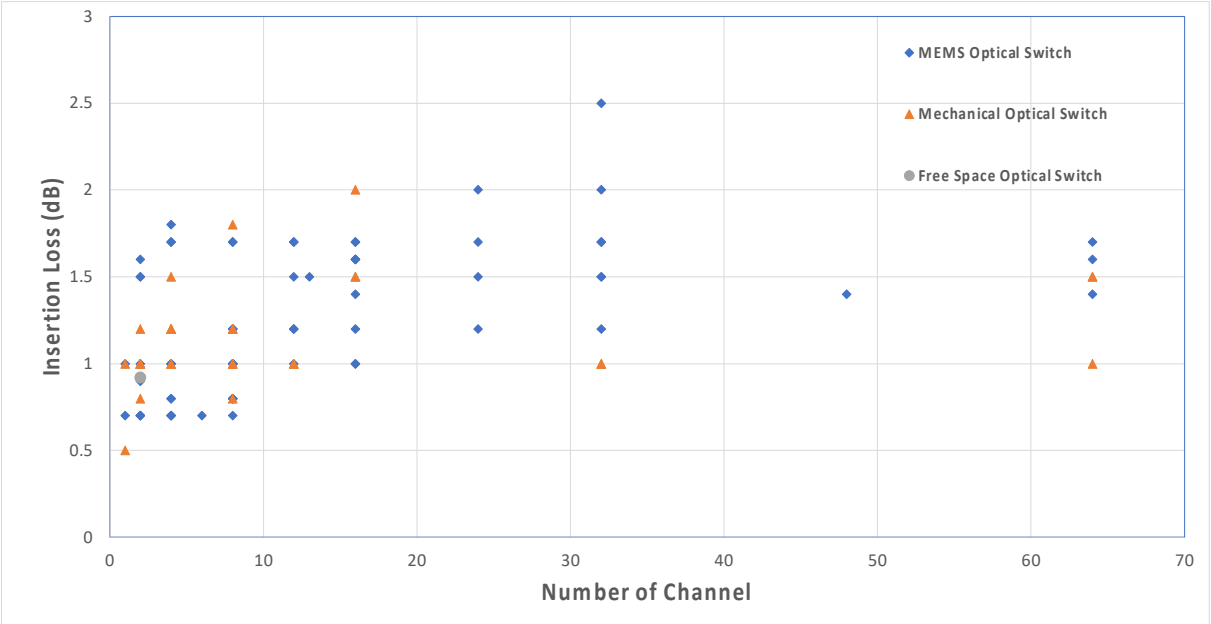

Fig. 2. Scatter plot of insertion loss versus number of quantum channels for three optical switches.

The blue diamonds are MEMS optical switches, the orange triangles are mechanical optical switches, and the grey circles represent the free space optical switches constructed in this paper using a galvo mirror system, with an insertion loss of about $0.92dB$. It can be seen from the figure that the trend of the insertion loss for the commercial MEMS optical switches and the mechanical optical switches is to increase with the increase in the number of quantum channels, from a minimum of$0.5dB$ to $2.5dB$. However, it is also noted that there are optical switches with lower insertion loss even when the number of quantum channels is as high as 64, and one possible explanation is that the optical switch does not directly connect the input ports to the 64 output ports but combines multiple 1×4 optical switches. Due to the limited sample searched and the fact that these optical switches are from different manufacturers, no significant difference in insertion loss is observed between the MEMS optical switch and the mechanical optical switch. The configured free-space optical switches have lower insertion loss compared to commercial optical switches. Due to the good scalability of free-space optical switches, it can be assumed that there is potential for further optimization. Also, this figure provides a research objective, for example, in studying the design of a 1×16 free space optical switch that needs to be designed so that its insertion loss is less than $1dB$.

Compared to commercial optical switches, free-space optical switches with macroscopic dimensions make it easier to adjust the distance so that the beam input to the optical switch achieves the optimal coupling distance. This figure also demonstrates that free space optical switches have the great potential for achieving very low insertion loss.

Chapter 3 The Characterization of Galvo Mirror System

Galvo mirror system is a common optical device that is often used for scanning or positioning of light beams. It consists of one or more galvanometers that control and adjust the direction and position of the beam by rapid vibration. Due to the small size and low inertia of the galvanometer, the system has a fast response time and can be operated accurately over a large working range, and is mostly used in laser scanning imaging, laser cutting, and optical scanning mirrors. In this chapter, the components of the galvo mirror system, its principle of operation, and several experiments characterizing its performance properties will be presented to confirm the feasibility of using the scanning galvanometer system to control the optical beam, and to provide guidance for the research and design of the optical router.

3.1 Galvo Mirror System

In this paper, a one-dimensional scanning galvo mirror system from Thorlabs is used, which consists mainly of the galvanometer, mirror, and servo driver board, as can be seen in Fig. 3. The main components of the galvanometer are a servo motor that controls the steering of the mirror and a detector that feeds back information about the position of the mirror. A galvanometer uses the motor effect to detect and measure a current in an electric circuit. When a current passes through its wires, it generates a magnetic field that repels the permanent magnet, thus driving the mirror to rotate.

Information about the position of the reflector is provided by a photodetector. The photodetector is used to detect the intensity of the light beam or other optical parameters, it converts the optical signal into an electrical signal and outputs a corresponding current or voltage signal.

Fig. 3. The GVSK1 Series Galvo Mirror System Kits.

A gold-coated mirror is mounted on the rotating axis of the galvanometer, which is connected to the driver board to move the beam within the angular range of the motor shaft. The whole system is controlled by proportional differential (PD), which controls the angle of the mirror by controlling the voltage. The specific process is as follows:

the servo driver board receives the feedback signal of position, compares the current position with the target position, and calculates the position error. According to the position error, the servo driver board generates the corresponding control signal, and sends it to the servo motor or actuator to apply the appropriate force or torque to the galvanometer.

Considering that the servo motor is a closed-loop system, which allows more precise control of the motor rotation speed and position compared to a normal stepper motor, the galvo mirror system is first considered as a component of the optical router in this project. Properties such as position accuracy and repeatability will be characterised to verify the feasibility of using this instrument to control the beam. In the configuration of this paper, the ratio between the input voltage and the position of the mirror is 1, and the mirror can move between $\pm 10°$ over a range of $\pm 10V$ input voltage.

3.2 Experimental Setup

The experimental setup is shown in Fig. 4. It can be regarded as a 1×1 free-space optical switch, in which the galvo mirror system is used to control the beam movement. A laser with a wavelength of $1310nm$ is used as a light source and input through a single mode fiber. Considering that the process of measuring the input power

will destroy the optical path, an optical beam splitter is used to split it into two beams of equal power, one of which passes through the reference input coupler and is measured by a photodetector to obtain the reference input power; The other beam is directed into a reflective collimator, where the beam in the fiber becomes collimated and emitted into free space. After reflection from the galvo mirror and the gold-coated mirror, the beam enters the output coupler and the collimated beam in free space is coupled into the single-mode fibre. Depending on the purpose of the experiment, the choice was made to use either a photodetector or a fast photodetector to measure the output power.

In this experimental setup, a reflective collimator with a focal length of $7\ mm$ is used to collimate and couple the beam, and the distance between the galvanometer and the output coupler is roughly set to $20\ cm$. The optical path was calibrated before the start of the experiment to roughly ensure that the optical path was aligned, the beam was incident from the end face of the fibre, and the centre of the beam waist was aligned with the centre of the fibre core, etc., so that the beam was hitting the centre of the galvanometer and the reflector.

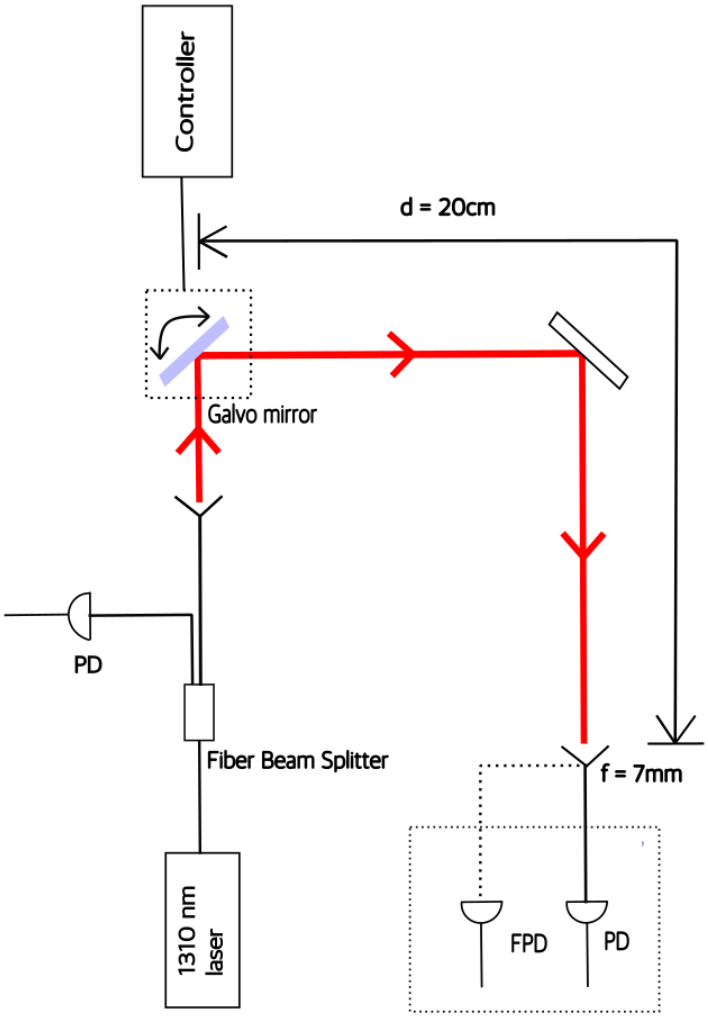

Fig. 4. Optical setup.

3.3 Experiment Results

Using the galvo mirror system as the part of the optical router that controls the beam requires consideration of beam coupling, positional accuracy, and dynamic characteristics of the system. In this section the properties of the galvo mirror system in this configuration will be explored, i.e., measurements were made of the acceptance

angle, the repeatability of the mirror position, the dynamic properties of the galvanometer movement, and the speed of the galvanometer movement, respectively.

3.3.1 Acceptance Angle

The input beam will enter the output coupler through the reflection of the galvanometer and gold-coated mirrors. The angle at which the beam is directed into the centre of the output coupler is set to 0°, and the degree is negative when the beam is deflected to the left and positive when it is deflected to the right. When the voltage changes, the galvanometer will adjust the angle with a ratio of 1.

As shown in Fig. 5 (a), the angle range of the beam into the output coupler is the acceptance angle θ. In order to determine when the beam will no longer be collected by the coupler, i.e., to measure the magnitude of the acceptance angle, the galvo mirror was deflected from -0.2° degrees up to 0.2°, during which a photodetector was used to measure the output power.

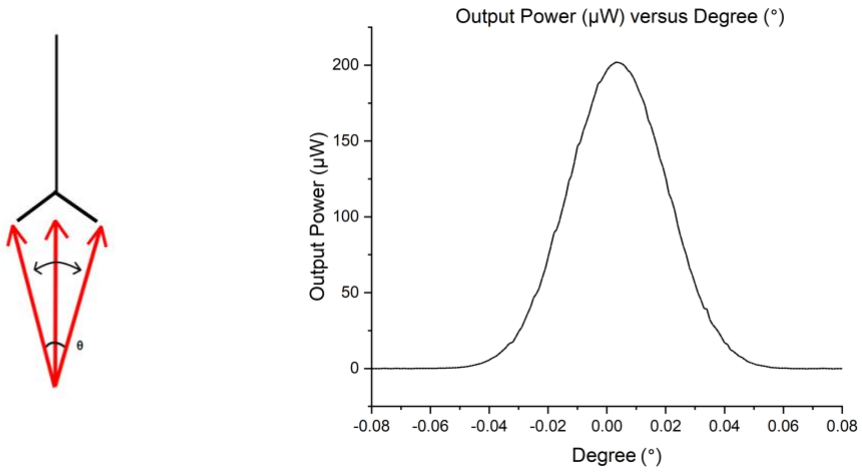

Fig. 5. Measurement of Acceptance Angle. (a) Acceptance Angle θ. (b) Curve of Output Power versus Degree.

The experimental results are shown in Fig.5 (b). The horizontal axis is the angle of beam deflection and the vertical axis is the output power. The output power is almost $0\mu W$ before $-0.05°$, from this degree, the output power increases with the angle, until near $0°$ when the curve reaches the peak, about $200\mu W$. After that the output power decreases as the angle increases until about $0.05°$, where the output power will drop to $0\mu W$. It can be seen that the beam can enter the coupler when the angle is deflected up to $-0.05°$, until after $0.05°$ the beam will not be collected by the coupler. The receptance angle is about $0.1°$.

This experiment measures the acceptance angle of the coupler. With the known acceptance angle and the ratio of the angle to the input voltage, the galvanometer can

be precisely controlled to move within the range of the acceptance angle in order to achieve effective beam coupling. It can also be used for system integration and layout design, i.e., to determine the position and orientation of the light source or optical components, and to provide guidance for the research and design of optical switches.

3.3.2 Repeatability of The Mirror Positioning

The repeatability of the mirror position reflects, to some extent, the accuracy and stability of the galvo mirror system to control the mirror position. To ensure that the optical router based on the galvo mirror system has a good positional accuracy, so this experiment will explore the repeatability of the galvanometer.

The position of the galvanometer at an angle of $0°$ was used as the reference position, and the position that could be moved was limited to that represented by an integer number of degrees between $-10°$ and $10°$. A photodetector was first used to measure the reference input power and output power when the galvo mirror was in the reference position. After the measurement, the galvanometer was moved to any random position within the specified range, and then the galvo mirror was controlled to return to the reference position for the next measurement. Make this process repeated 1000 times, the results are shown in Fig. 6.

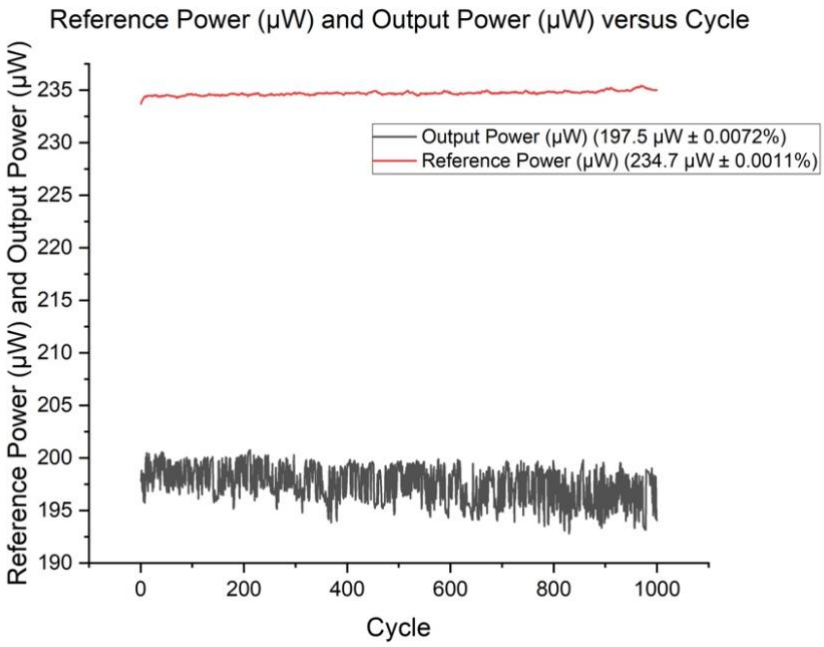

Fig. 6. Variation of reference power and output power with the number of cycles

The horizontal axis is the number of cycles, the vertical axis is the power, and the red curve located at the top of the image represents the reference input power and the black curve at the bottom represents the output power. According to the image, the curve of the reference input power is flat and the value of the power does not change significantly between the approaching cycles, which is about $234.7\mu W$. However, the output power curve oscillates back and forth, representing some drift in the mirror position. A more plausible explanation is that since the galvanometer is current driven, if there is a slight change in the reference current within the galvo mirror system, the position of the mirror will change as well. And the output power is significantly lower than the reference output power, which is about $197.5\mu W$. There is a slight increase in

the amplitude of the oscillation of the output power curve as the number of cycles becomes higher. This may be due to the fact that the reference current has drifted in the first experiment. In subsequent experiments, this error will be superimposed, so that the noise in the curve below the image is gradually increasing.

3.3.3 Dynamic of mirror movement

The dynamic of a galvo mirror system are the response and behavior of the system during galvo mirror motion. In this system, the position of the mirror will be adjusted by controlling the voltage. Errors, drifts or vibrations in the system can be monitored by studying the dynamic of the mirror movement. Based on the experimental results, drive signals can be adjusted or correction algorithms can be applied to achieve the desired accuracy and stability.

This experiment focus on exploring how the galvanometer moves to determine if the galvo mirror system is tuned. The position of the galvo mirror at a voltage of $0V$ was set as the test voltage position. A total of two experiments were conducted: using a fast photodetector to measure the signal during the movement of the mirror to the test voltage position and the mirror moving away from the test voltage position, respectively, and the results of the experiments are shown in Fig. 7 (a) and (b).

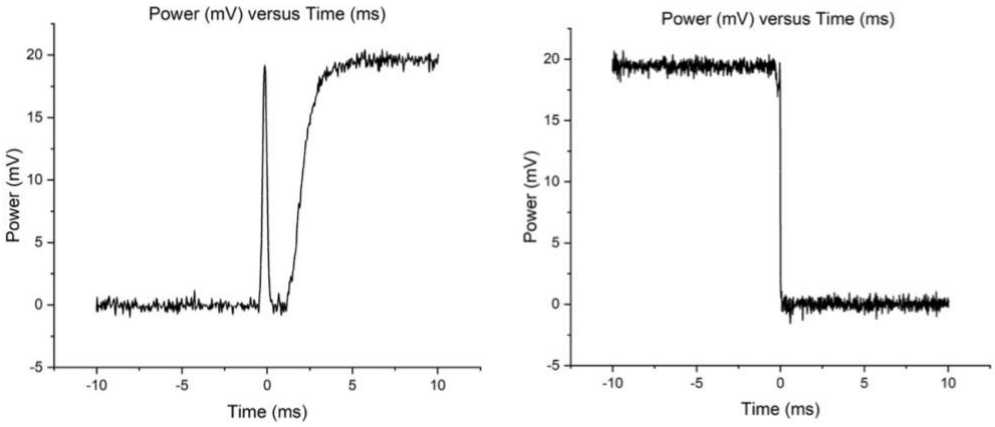

Fig. 7. (a) the mirror moves towards the position close to the test voltage. (b) the mirror moves away from the test voltage.

Fig. 7 (a) shows the curve of voltage signal over time as the mirror moves towards the test voltage position. There is a large peak at $0ms$. The voltage then gradually increases with time from $0mV$ and reaches about $20mV$ at about $5ms$. The peak at 0ms means that the mirror is moving with underdamping due to system overshoot. After about $3ms$, the galvo mirror reaches the test voltage position and the voltage signal tends to be stable. Fig. 7 (b) shows the voltage signal over time as the mirror is removed from the test voltage position. The voltage stabilizes at about $20mV$ before $0ms$ and then drops abruptly near $0ms$, but a small peak can be observed at the beginning of the curve drop, followed by a drop to $0mV$. This is because the galvo mirror suddenly turns in the opposite direction while moving away from the test voltage position, and then returns to the correct direction within a short period of time.

The experiments show that the galvo mirror overshoots or drifts during movement. But because the system is managed by the PD controller, which provides a control operation based on feedback derived from the error, the galvanometer is shifted to the desired direction and continues to move towards the set position.

3.3.4 Speed of the Mirror Movement

The speed of the mirror movement directly affects the speed and response time of the system. The faster the galvanometer moves, the faster the system can position and scan the beam, which leads to faster data processing and acquisition rates. To give thorough evaluation of the features of the galvo mirror system, this experiment will investigate the speed of the mirror movement.

The test voltage position is also set at $0V$. The galvo mirror is set up to sweep the test voltage point and the voltage is measured with a fast photodetector. As shown in Fig. 8, the output voltage varies with time. The voltage rises and reaches a peak close to $0ms$, after which it falls to $0mV$. From this figure, it can be concluded that the time required for the mirror to sweep through the test voltage point is about $0.015ms$, and from Fig. 5 (b), the acceptance angle is about $0.1°$, so the speed of the mirror movement can be calculated, which is about $6.67°/ms$.

Notably, quick reconfiguration is of secondary relevance since typical quantum communication activities might range from a few seconds to many hours, thus this is not a very crucial quality for quantum key distribution. In this project, the speed of the mirror movement is therefore measured for its possible applications in order to more thoroughly characterize the characteristics of the galvo mirror system.

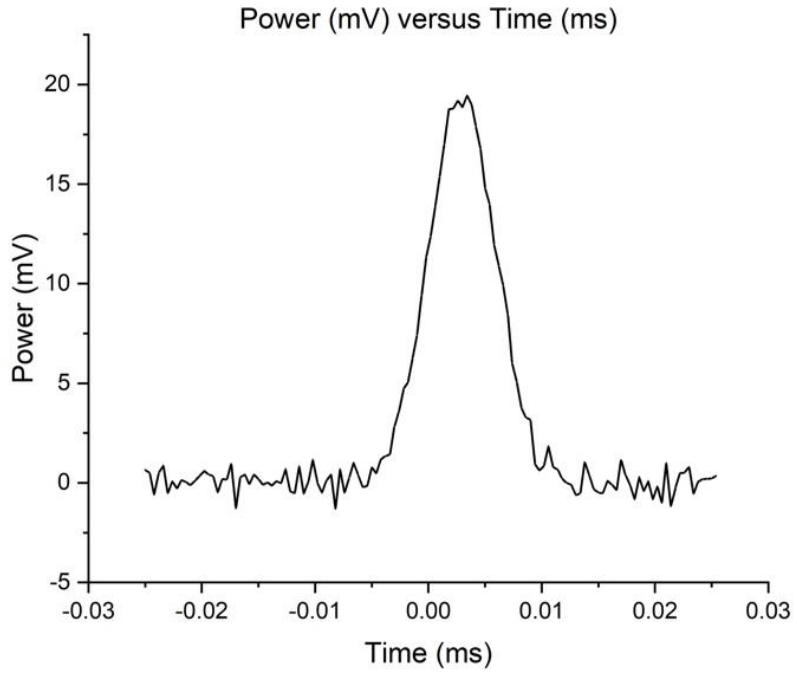

Fig. 8. Image of output voltage over time.

3.4 Summary

This chapter introduces the experimental setup and the working principle of the galvo mirror system. It also provides an analysis of the system's acceptance angle,

positional accuracy, dynamic, and response speed. It was discovered that the acceptance angle of the reflecting collimator was roughly 0.1°. When characterizing the repeatability of the mirror movement, it was found that the mirror had a certain drift and would not reach the specified position precisely every time, which was responsible for the up and down oscillation of the image. It was discovered that the signal was overshooting during the dynamic analysis of the mirror movement. However, because the PD controller's feedback mechanism was in place, the control system was able to return the movement to its predetermined trajectory. It was also measured how quickly the mirror moved; the result was roughly $6.67°/ms$.

The process of characterizing the galvo mirror system yields valuable insights into its behavior and properties, as well as performance metrics and parameters that can be used to assess the system's stability, reliability, and practicality. These insights can then be used to inform the design and optimization of optical routers.

Chapter 4 Optimization of the fiber-to-fiber free-space coupling

For free-space optical switches, the laser in a single-mode fibre enters the free space after being collimated by an optical collimator, passes through a reflector or other optics, and finally enters an optical coupler and is coupled into the fibre. To optimize the fibre-to-fibre free-space coupling, in this chapter the beam waist will be measured to characterize different classes of optical collimators. The optimal configuration of the fibre-to-fibre free-space coupling will be explored, including the choice of collimator and the optimal coupling distance from the fibre to the collimator and from the collimator to the collimator.

4.1 Optical Collimator

4.1.1 Reflective Collimator

The focal length of the mirror remains constant over a wide range of wavelengths. Due to this inherent characteristic, reflective collimators do not need to be adjusted for different wavelengths of light and can be used in systems where multiple wavelengths need to be collimated or systems where polychromatic light needs to be coupled. Reflective collimators are preferred in the selection of optical collimators. The reflective collimator is shown in Fig. 9. The beam entering the reflective collimator is reflected by the mirrors, and the diverging beam becomes a parallel beam and is output into free space.

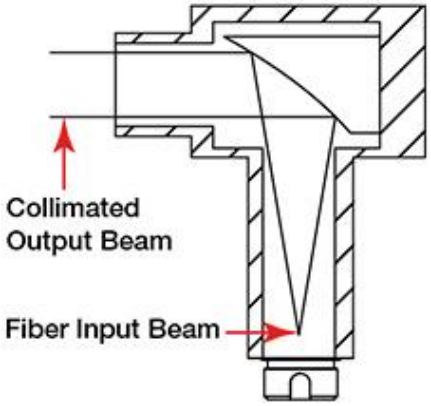

Fig. 9. Schematic diagram of the reflection collimator[1].

4.1.2 GRIN Collimator

Graduated refractive index (GRIN) lenses are cylindrical optical lenses in which the refractive index decreases radially to focus or collimate the beam. GRIN lens fibre optic collimator/coupler coupled with a standard single-mode fibre; the GRIN lenses are held in stainless steel housings and are generally used in pairs, coupling a free-space beam between the two lenses, as shown in Fig. 10.

[1] Source: Thorlabs

Fig. 10. Pair of GRIN collimators[2].

The range of distance between the two collimators, i.e., the operating range, is limited to 5 ± 15 mm, where the maximum coupling efficiency can be obtained. For this subject, the operating range of the GRIN collimator is too small, which means that it is not possible to add mirrors or other optics between the two collimators, and therefore it is not suitable as a collimator in free-space optical switches.

4.1.3 Aspheric Collimator

An aspheric collimator is a collimator that uses an aspheric lens to collimate the beam. An aspherical lens collimates the beam without introducing spherical aberration in front of the transmitted wave, and is a correction for a spherical lens. It varies in curvature from the centre to the edge, with less curvature the closer to the edge of the

[2] Source: Thorlabs

lens. Spherical aberration causes the light source to fail to converge into a point after passing through the spherical lens and only a fuzzy diffuse spot is formed, making the spherical lens unable to achieve diffraction-limited performance when collimated.

4.2 Beam Waist Measurement

4.2.1 Experimental Setup

By measuring the Gaussian beam diameter, information about the beam profile and the position and size of the beam waist can be obtained. The coupling efficiency is maximized when the beam waist of the collimated beam is in the middle of the two couplers. In this section, the experimental setup for beam waist measurement is described.

The most popular techniques for measuring the laser's beam diameter are the pinhole, CCD, and knife-edge methods. Since the pinhole method is difficult to ensure the accuracy; the CCD method is highly accurate, but only applies to low-power beam measurements; and the knife-edge method is suitable for high-power beam diameter measurements[11], so this paper adopts the knife-edge method to measure the diameter of the Gaussian beam. The knife-edge method works as follows: when the blade does not block the beam, the power detected by the optical power meter is maximum; as the blade moves horizontally or vertically in the direction of the blocking beam, the blade

cuts the beam and the power gradually decreases; until the blade completely blocks the beam and the power reaches a minimum value.

The experimental setup is shown in Fig. 11 (a) and (b). The beam in the single mode fibre is passed through the optical collimator into free space and is detected by a photodetector. The device for fixing and controlling the blades is placed at a distance $x(cm)$ from the optical collimator, this distance can be measured by means of a ruler. Two blades perpendicular to each other, one parallel to the x-axis and one parallel to the y-axis, are fixed together to cut the beam from the horizontal and vertical directions, respectively, as shown in Fig. 11 (b). In the experiment, the blade was first controlled to move in a positive direction towards the y-axis until the beam was completely uncovered. The blade was moved horizontally in the negative direction of the x-axis until the blade completely blocked the beam. The power output was measured to obtain the diameter of the beam in the x-axis at this distance. The blade position was then restored to the position at the beginning of the experiment, and the blade was moved in the positive direction of the y-axis until the beam was not blocked at all. The diameter of the beam in the y-axis at this distance was obtained. The first measurement is taken when the blade is very close to the collimator (about 1-$5cm$), and measurements are taken every $5cm$ between them. The experimental results were fitted to obtain the beam profile and the size and position of the beam waist.

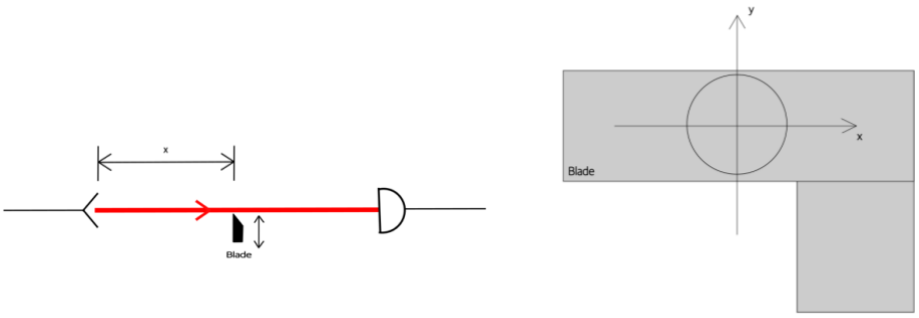

(a) (b)

Fig. 11. Schematic diagram of the setup for the knife-edge method.

4.2.2 Measurement results

The experiment was first carried out using a reflective collimator. The distance between the device holding the blade and the collimator was made to range from $5cm$ and $30cm$, and measurements were taken at $5cm$ intervals for a total of five measurements. Four reflective collimators with a reflective focal length (RFL) of 7 mm were characterized and the beam profile is shown in Fig. 12.

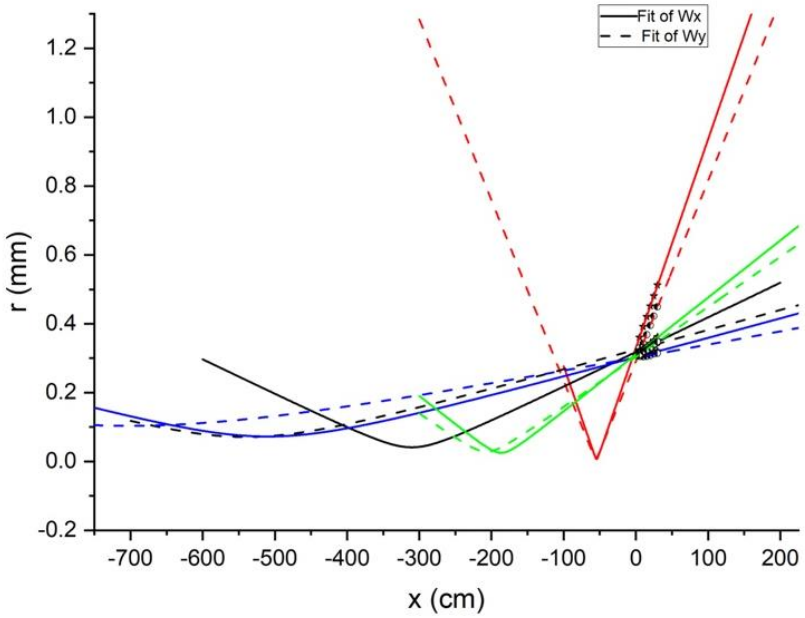

Fig. 12. Beam profile of the reflective collimators.

The curves of different colors represent the beam profiles passing through different collimators, the solid line shows the fitted curve obtained by cutting the beam in the horizontal direction of the blade and the dashed line shows the fitted curve obtained by cutting the beam in the vertical direction of the blade. The points in the figure concentrated in the range of $5cm$ to $30cm$ are the data obtained through experiments. The lowest point of the curve is the beam waist. The closer the curve of the x-axis and y-axis of the same reflective collimator is, the closer the beam diameter is in the x-axis and y-axis, and the incident beam can be regarded as a normal incidence from the fibre end face, which makes the coupling efficiency higher.

The full angle beam divergence of the Gaussian beam can be calculated from the beam profile, as shown in Table 1.

Table 1. The full angle beam divergence between x-axis and y-axis of reflective collimator.

Reflective collimator	Full Angle Beam Divergence of x-axis (°)	Full Angle Beam Divergence of y-axis (°)
1	0.068	0.07
2	0.012	0.006
3	0.003	0.004
4	0.018	0.016

It is mentioned in Thorlabs that the reflective collimator used in the experiment had a full angle beam divergence of $0.2°$, then comparing this to the data calculated in the table, the collimators all met the criteria. However, it is obvious from the beam profile that the curve is divergent. So, an experiment was attempted to change to a reflective collimator with an effective focal length of $33mm$ to measure the diameter of the beam at a distance between $5cm$ and $40cm$. The experimental results indicate that the variation of the beam diameter in this interval is small enough that a curve

cannot be fitted. However, due to the limitations of the table size, it was not possible to measure the beam diameter at longer distances. Also, the measured beam waist diameter was around $3.5mm$.

The beam output from a reflective collimator with an effective focal length of $7mm$ is divergent, and the beam output from a collimator with an effective focal length of $33mm$ can be regarded as collimated, but with a larger beam diameter. However, since the focal length of the reflector is strictly determined and cannot be further optimised, a collimating lens is considered as a coupler for the optical switch, and the collimating lens is characterized next.

A molded glass aspherical lens was used for the experiment. A single mode optical fibre is connected to a fibre adapter fixed to a XY translation mount. It can be manually adjusted in the XY direction so that the light beam is accurately directed into the aspherical lens. The lens is fixed in the Z-axis translation mount and can be manually adjusted in the Z-axis direction. Since the XY translation mount and the Z-axis translation mount are compatible with the $30mm$ cage system, they can be connected to form a collimator, as shown in Fig. 13. After roughly adjusting the distance from the lens to the fibre, the spot in free space near the collimator and farther away are compared by visual observation. If the beam diameters at the two positions are almost

the same and the spot is bright and clear, then the beam divergence is low at this position. The beam diameter is measured after adjusting the optical path.

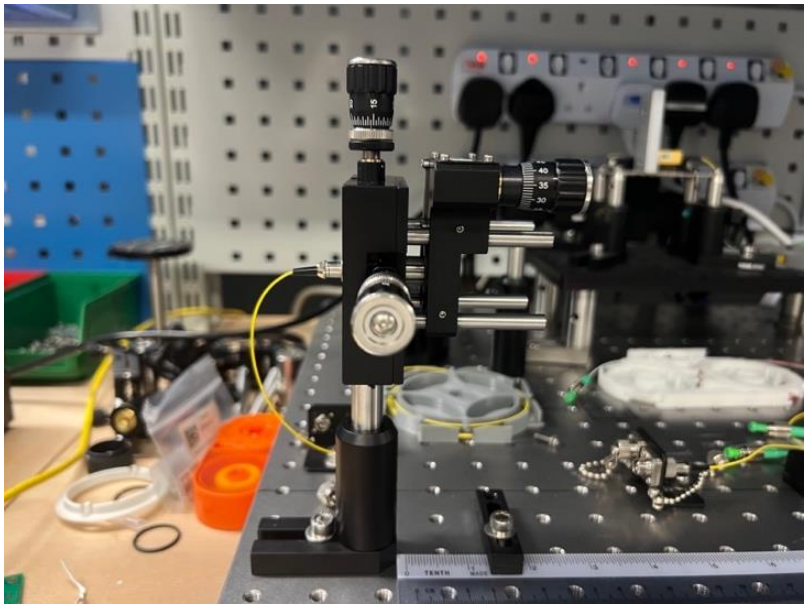

Fig. 13. Collimator made with molded glass aspheric lens.

Fig. 14 shows the beam profile of a C230TMD-C lens. The green curve represents the beam profile in the horizontal direction, with the beam waist at approximately $-47cm$ and a beam radius of about $0.0091cm$. The yellow curve represents the beam profile in the vertical direction, with the beam waist at approximately $-36cm$ and a radius of roughly $0.00761cm$.

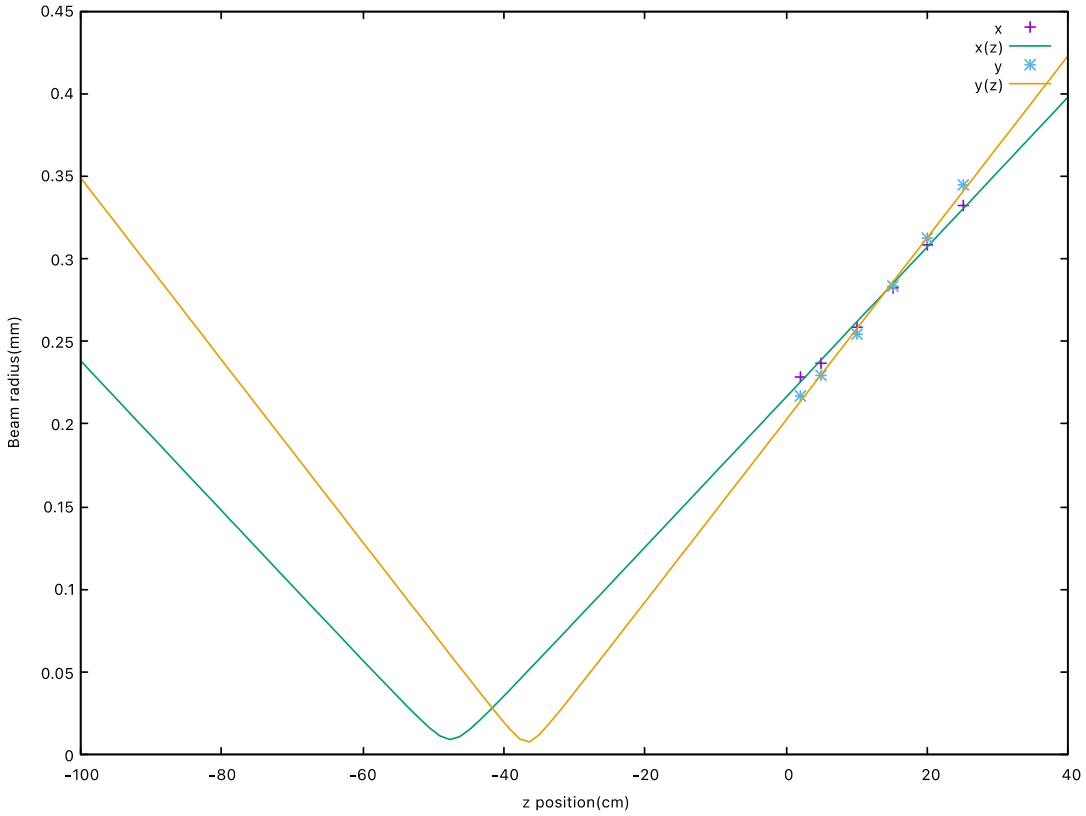

Fig. 14. Beam profile of the C230TMD-C lens.

4.3 Optimization of Experiment setup

In the previous scenario, we need to characterize two collimators to find the best distance between them, which makes their beam profiles match each other. However, it was found in the experiments that it was not easy to find the right distance. So, we tried to simplify the measurement by using a circulator. The optimized experimental setup is shown in Fig. 15.

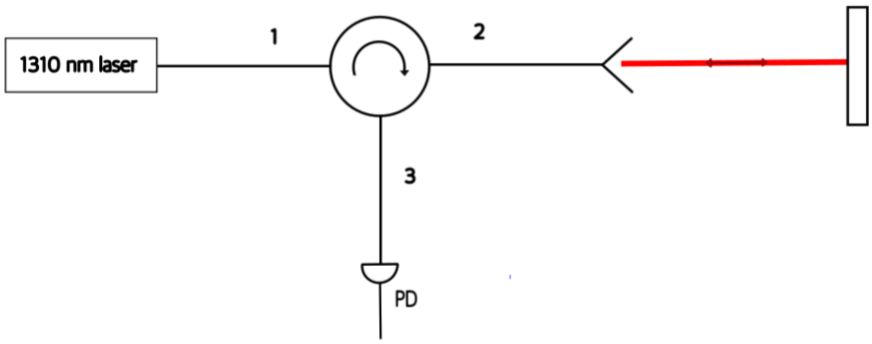

Fig. 15. The optimized experimental setup.

The circulator specifies that beams entering from port 1 can only be output from port 2; beams entering from port 2 can only be output from port 3. This loop is not reversible. In the experiment, a $1310\,nm$ laser is input from port 1 and output from port 2 into free space. The beam that is vertically reflected by the mirror enters port 2 and is finally output from port 3. After adding the circulator to the experimental setup, only one collimator needs to be characterized, while the other collimator is replaced by a mirror.

4.4 Discussion

In this chapter a variety of collimators are mainly characterized. For reflective collimators, the advantage is that the focal length does not change with wavelength.

However, due to the measured beam profile showing a more divergent beam, and because the focal length is strictly determined, no further optimization of this collimator is possible. Then we moved to the lenses. For GRIN lenses, free-space coupling is suitable, but the working distance is too small to place optics between two collimators. For the aspherical lens, the diameter of the beam passing through the C230TMD-C lens was measured, and the measurements showed that the beam was divergent. Thus, to simplify the experiment, a circulator was added to the experimental setup, which will be further characterized in subsequent experiments.

Chapter 5 Conclusion and Future Work

5.1 Conclusion

This paper focuses on the feasibility of using free-space optical switches to optimize quantum communication.

The first part introduces mechanical optical switches and MEMS optical switches, and compares the insertion loss of commercial optical switches with that of free-space optical switches. The loss of the configured free-space optical switch is about $0.92\ dB$. The commercial optical switch has comparable insertion loss with the free-space optical switch, and the use of the free-space optical switch makes sense when the number of output channels is large.

The second section describes the galvo mirror system, experimentally characterizing the acceptance angle, positioning accuracy, repeatability and dynamic properties.

The third section analyses reflective collimators, GRIN lenses, and aspherical lenses. The diameter of the beam after passing through the collimator is measured using the knife-edge method to obtain the beam profile and beam waist position. Afterwards,

the experimental setup was simplified by adding a circulator to the experimental setup, and we only needed to characterize one collimator.

5.2 Future Work

The characterization of the lenses will be further refined in the future. In addition, optimization of quantum traffic with WDM will be considered as free-space optical switches and commercial optical switches have comparable insertion losses.

This is a research area full of challenges and opportunities. By continuously improving the scalability, stability and noise suppression of optical routers, we are expected to achieve more efficient and reliable quantum communication networks. This may bring an important boost to the development and practical application of quantum communication technology and play a role in the future information and communication field.

Appendix A Insertion Loss

Insertion loss is the power loss of a signal during transmission through an optical device or fibre. In optical communication systems, insertion loss is an important performance parameter that measures the degree of attenuation of the optical signal during transmission. The size of the insertion loss directly affects the transmission quality and distance of the system and is usually expressed in decibels (dB). If the power transmitted to the input is P_{in} and the power received at the output is P_{out}, the insertion loss (in dB) is:

$$1L(dB) = -10 \log_{10} \frac{P_{out}}{P_{in}} \quad (1)$$

Insertion loss can be caused by a variety of factors, including material loss in the optics, attenuation of the optical fibre, and imperfect matching of connectors and connecting splices. The material loss of the optical device is mainly caused by the absorption and scattering of the material itself, while the attenuation of the optical fibre is due to the loss of the optical signal with the optical fibre material in the transmission process. Some measures can be taken to reduce the loss, such as selecting low-loss optical devices or replacing the fibre optic medium with an air medium. In quantum communication, the insertion loss needs to be reduced as much as possible to ensure the signal transmission quality and system performance.

Therefore, it is very important to accurately assess and control the insertion loss during system design and implementation.

Appendix B Gaussian Beam

Gaussian beam (Gaussian Beam) is a special type of beam, the main feature is the transverse intensity distribution in the form of a Gaussian function, that is, in the transverse direction of the light intensity of the normal distribution curve, the middle of the brightest, to the sides of the gradual weakening. The intensity distribution of a Gaussian beam can be described by a series of mathematical formulas:

$$I(r,z) = I_0 \left[\frac{W_0}{W(z)}\right]^2 exp\left[\frac{-2r^2}{W^2(z)}\right] \tag{2}$$

$$W(z) = W_0 \sqrt{1 + \left(\frac{z}{z_0}\right)^2} \tag{3}$$

$$z_0 = \frac{\pi W_0^2}{\lambda} \tag{4}$$

The beam radius changes with the direction of propagation, $W(z)$ is a function of the beam width measured along the direction of propagation, r is the beam radius of the beam at z, and W_0 represents the beam waist radius. z_0 represents the Rayleigh range, defined as the distance behind the focal point of a beam during free propagation, i.e., after the Rayleigh range, the beam begins to diverge. The Rayleigh range is mainly used to describe the focusing nature of the beam and the size of the spot. Fig. 16 depicts the curve of the beam radius of a Gaussian beam as a function of the direction of propagation.

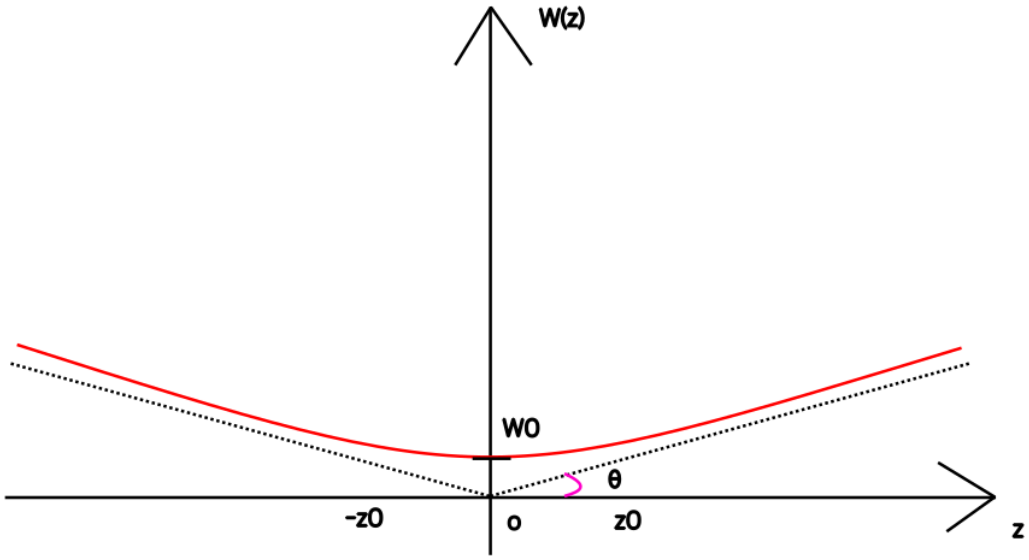

Fig. 16. Beam Profile of a Gaussian Beam.

In addition, the divergence angle θ indicates the range of angles at which the beam diverges from the light source or focal point, and is a physical quantity that describes the degree of diffusion of the beam. The larger the divergence angle, the more obvious the beam diffusion. The formula is as follows:

$$\theta = \frac{\lambda}{\pi w_0} \tag{5}$$

Appendix C PID controller

A Proportional-Integral-Differential controller (PID controller) is a control loop mechanism that uses feedback and consists of a Proportional, Integral and Derivative unit. It is widely used in industrial control systems and a variety of other applications that require continuously modulated control. The PID controller is shown in Fig. 17. The function of the setpoint SP is $r(t)$ and the function of the process variable is $y(t)$, and the controller continuously calculates the error $e(t) = r(t) - y(t)$ as a function of the measured results and the setpoint. Using the error function based on the PID algorithm to get the corrected value to the system and make it as a new input to reduce or even eliminate the error of the system measurement.

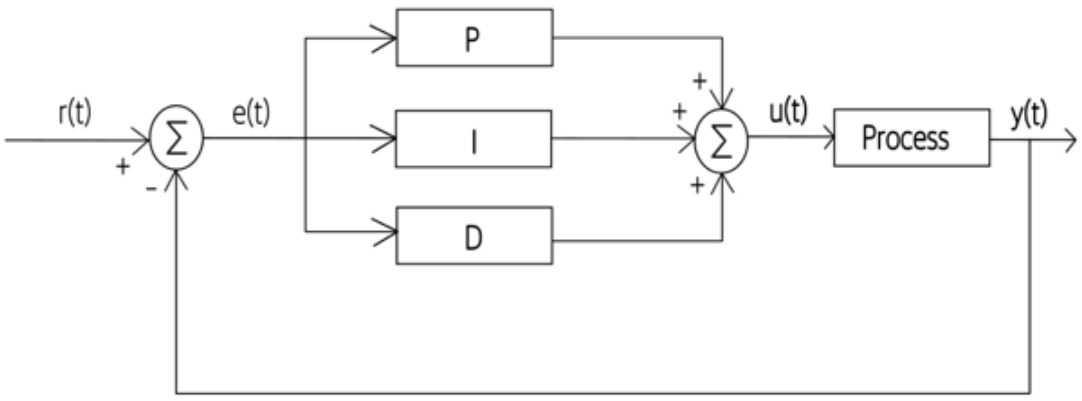

Fig. 17. PID Controller.

In the PID loop, there are three algorithms for correcting the value: the proportional part calculates the output signal based on the current deviation, the integral part calculates the output signal based on the cumulative deviation over the past period of time, and the differential part calculates the output signal based on the rate of change of the current deviation, and the result of the three algorithms when added together is the corrected value. Defining $u(t)$ as the control output, the PID algorithm can be expressed by the following equation:

$$u(t) = K_p e(t) + K_i \int_0^t e(\tau)d\tau + K_d \frac{d}{dt} e(t) \tag{6}$$

The P term is proportional to the current SP-PV error value, e.g., when the error is large, the control output is increased proportionally using K_p. Item I is obtained based on the accumulated value of SP-PV error in the past period of time, if SP-PV error still exists after proportional control, this item is used to eliminate the steady state error and ensure that the system meets the desired value in a long period of time. item D is based on the rate of change of the current error to calculate the output signal, which is adjusted by the trend of the change of the SP-PV error to achieve the fast stability of the system and suppress the overshooting control. overshooting control. The faster the change, the greater the control or damping effect.

PID three units can not be applied at the same time, for example, in this paper, the galvo mirror system, only need to use the PD controller, then you can set the unit parameter of I that does not need to be used to 0.

Reference

1. BENNETT C H. Quantum cryptography: Public key distribution and coin tossing. Proc of IEEE International Conference on Computers Institute of Electrical and Electronics Engineers, 1984.
2. WOOTTERS W K, ZUREK W H. A Single Quantum Cannot be Cloned[J]. Nature 299, 1982. pp. 802–803.
3. Shen Hong, Ma Changchao, Han Peng et al. Frontier report on the development and application of quantum secure communication technology [R]. Communications Society of China, 2020.
4. Hou Jia, Zhu Jiang. Research on quantum key distribution network scheme[J]. Communication Technology, 2021, 54(06): 1291-1300.
5. P. D. TOWNSEND, I. THOMPSON. A Quantum Key Distribution Channel Based on Optical Fibre[J]. Journal of Modern Optics, 1994. 41: 12, 2425-2433.
6. ELLIOTT, CHIP. Building the quantum network[J]. New Journal of Physics, 2002, 4: 46.
7. BRIEGEL H J. Quantum repeaters: the role of imperfect local operations in quantum communication[J]. Physical Review Letters, 1998, 81: 5932-5935.
8. Wang Hua, Zhao Yongli. Quantum key distribution metropolitan optical networking technology foresight[J]. Journal of Communications, 2019, 40(09): 168-174.
9. Cao J.-Z. Performance analysis of mechanical optical switch[J]. Tianjin

Communication Technology, 2004, (02): 21-24.

10. Hu Jian, Li Gangyan. Research on optical switching technology based on MEMS [J]. Semiconductor Technology, 2007, No. 224(04): 342-344.

11. Fan XM, Zheng Y, Sun QB et al. Experimental study of 90/10 knife-edge method for measuring beam waist of laser Gaussian beam[J]. Laser and Infrared, 2008, No. 357(06): 541-543.